Dynamical properties of quantum many-body systems with long-range interactions

Menghan Song, Jiarui Zhao,* Chengkang Zhou,† and Zi Yang Meng‡
Department of Physics and HKU-UCAS Joint Institute of Theoretical and Computational Physics, The University of Hong Kong, Pokfulam Road, Hong Kong SAR, China

(Received 8 January 2023; revised 15 May 2023; accepted 17 May 2023; published 25 July 2023)

Employing large-scale quantum Monte Carlo simulations, we systematically compute the energy spectra of the two-dimensional (2D) spin-1/2 Heisenberg model with long-range interactions. With the $1/r^{\alpha}$ ferromagnetic and staggered antiferromagnetic interactions, we find the explicit range in α for the short-range Goldstone-type (gapless), anomalous Goldstone-type (gapless), and Higgs-type (gapped) spectra. Accompanied by the spin-wave analysis, our numerical results vividly reveal how the long-range interactions alter the usual linear and quadratic magnon dispersions in 2D quantum magnets and give rise to anomalous dynamical exponents. Moreover, we find the explicit case where the gapped excitation emerges at a noninteger decay exponent α for the antiferromagnetic Hamiltonian. This work provides the first set of unbiased dynamical data of long-range quantum many-body systems and suggests that many universally accepted low-energy customs for short-range systems need to be substantially modified for long-range ones, which are of immediate relevance to the ongoing experimental efforts from quantum simulators to 2D quantum moiré materials.

DOI: 10.1103/PhysRevResearch.5.033046

I. INTRODUCTION

Quantum many-body systems with long-range (LR) interactions exhibit different and exotic properties compared with their short-range cousins, as the LR nature of the interaction differentiates them from many universally accepted long-wavelength and low-energy customs governing the short-range ones over the years. For example, the well-known Hohenberg-Mermin-Wagner theorem [1,2] that forbids spontaneous symmetry breaking of continuous symmetry at finite temperature in low dimensions can be easily circumvented and LR interactions can generate interesting finite-temperature transitions [3–9] and new critical phenomena [10–15]. The bedrock in the research of highly entangled quantum matter—the area law scaling of the entanglement entropy—can also be bypassed in LR systems, and the consequent new scaling behavior points towards a new guiding principle of quantum entanglement that needs to be worked out [8,16–21].

Moreover, recently the field of LR quantum-many-body systems becomes even more active due to their fast experimental realizations, such as the Rydberg atom arrays with long-range van der Waals or dipolar couplings where topological ordered phases, emergent glassy behavior, and quantum criticality have been suggested and realized [22–26], magic angle twisted bilayer graphene (TBG), and two-dimensional (2D) quantum moiré materials in which flat-band topology and long-range Coulomb interaction give rise to a plethora of correlated phases beyond semiclassical or band-theory description [27–69], as well as the quantum gases coupled to optical cavities [70] and programmable quantum simulators [26,71–75].

Despite such fast developments, theoretical and numerical investigations on the dynamical properties of the LR quantum many-body systems are still lacking. This is mainly due to the fact that dynamical properties, such as spectral functions [63,76–84], are usually difficult to compute without approximation in analytic theory and numerical simulations, even for the short-ranged systems. And therefore by now there exist few perturbative works such as Refs. [85–89], which are mainly valid at various mean-field limits where the fluctuations are suppressed, and previous algorithmic developments in nonperturbative numerical approaches for the LR system are mainly focused on classical and one-dimensional (1D) systems [90,91]. However, in the aforementioned experiments of 2D quantum LR systems, it is actually the dynamical information that can be easily detected by means of neutron scattering, nuclear magnetic resonance, scanning tunneling spectroscopy, nonlinear and nonequilibrium transport, and optical probes, etc.

To overcome the dilemma between the fast experimental developments and the slow theoretical reality in LR quantum many-body systems, the need to develop and carry out unbiased approaches, such as large-scale quantum Monte Carlo (QMC) simulations, to systematically investigate the dynamical properties therein is obvious. And only in this way can one fully reveal the interplay between the LR interaction and quantum topology and fluctuations to

*jrzhao@connect.hku.hk
†zhouchk@connect.hku.hk
‡zymeng@hku.hk

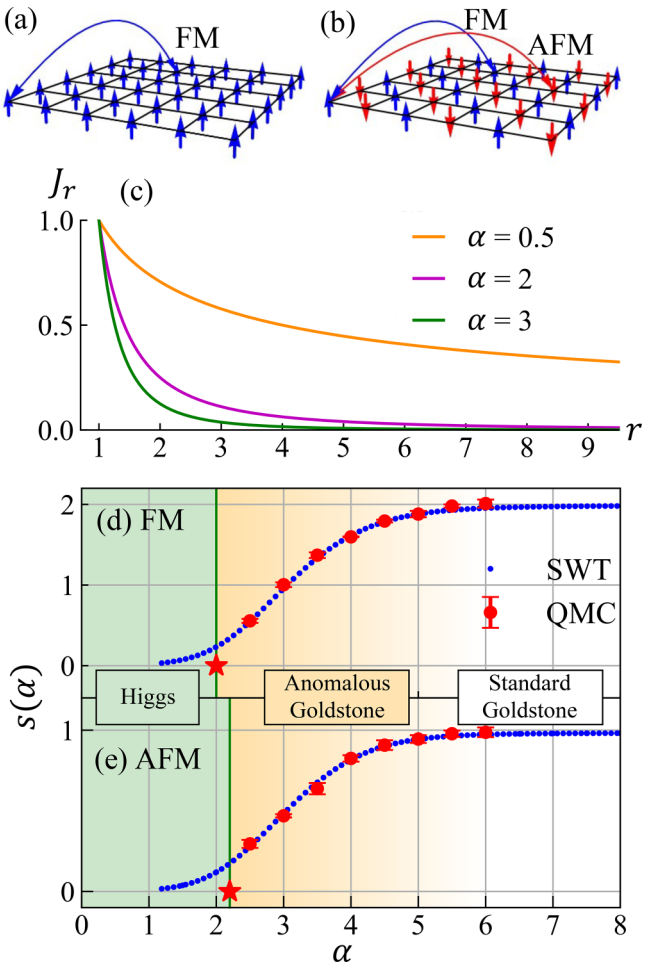

FIG. 1. 2D LR Heisenberg models with Higgs, anomalous, and short-range Goldstone spectra. The schematic plots of 2D Heisenberg model with LR ferromagnetic interaction (a) and staggered antiferromagnetic interaction (b). The power-law decay of $J(r) \sim 1/r^{\alpha}$ for three different α is shown in (c). (d, e) The power $s(\alpha)$ of low-energy spectra $\omega \sim |\mathbf{q}|^{s(\alpha)}$ obtained from QMC and SWT vs α for both the ferromagnetic and antiferromagnetic cases. The green-shaded area represents the Higgs regime where the spectra are gapped, the yellow-shaded area represents the anomalous Goldstone regime where the dispersion powers change with α, and the white area is the standard short-range Goldstone regime where $s = 1$ for antiferromagnetic and $s = 2$ for ferromagnetic cases. The red dots are fitting results from QMC ($L = 64$), and the red stars denote QMC boundaries at $\alpha = 2$ (for ferromagnetic) and $\alpha = 2.2$ (for antiferromagnetic), which separate the Higgs and Goldstone regimes. The blue dashed lines are fitting results from SWT, with a cutoff of longest coupling distance $r_{\max} = 1000$.

explain the fascinating experimental outcomes and predict new ones.

This is the focus of our paper. Here we develop and employ the stochastic series expansion (SSE) QMC [26,83,92,93] simulation for the LR quantum many-body systems to compute the energy spectra of the 2D spin-1/2 Heisenberg model with $1/r^{\alpha}$ interaction where α is the decay exponent, as shown in Fig. 1. With the interaction types of ferromagnetic [see Fig. 1(a)] and antiferromagnetic [staggered without introducing frustration, Fig. 1(b)], we find the explicit range in α for the short-range Goldstone-type (gapless), anomalous Goldstone-type (gapless but with varying dynamical exponent), and Higgs-type (where the spectra are gapped) spectra. As shown in Figs. 1(d) and 1(e), accompanied by spin-wave theory (SWT) analysis [12,94–98], our results reveal how the long-range interactions induce a mass to the Goldstone mode via the generalized Higgs mechanism [85]. Moreover, different from the conventional wisdom for systems with long-range interactions [88,99–101], we find an explicit case—the staggered antiferromagnetic model—where the gapped excitation exists even when the Hamiltonian is extensive. Therefore our work provides the first set of unbiased dynamical data of LR quantum many-body systems where universally accepted low-energy physics are substantially modified. Implications of ongoing experiments in quantum simulators and 2D quantum moiré materials are discussed.

II. MODEL AND METHOD

We consider the 2D spin-1/2 LR Heisenberg model with power-law decaying couplings on the square lattice. The Hamiltonians for the ferromagnetic (FM) and the antiferromagnetic (AFM) cases (with staggered interaction to avoid the sign problem [102,103]) are given by

$$H_{\mathrm{FM}} = -J \sum_{i \neq j} \frac{1}{|\mathbf{r}_i - \mathbf{r}_j|^{\alpha}} \mathbf{S}_i \cdot \mathbf{S}_j, \tag{1}$$

$$H_{\mathrm{AFM}} = J \sum_{i \neq j} \frac{(-1)^{|x_i + y_i - x_j - y_j + 1|}}{|\mathbf{r}_i - \mathbf{r}_j|^{\alpha}} \mathbf{S}_i \cdot \mathbf{S}_j. \tag{2}$$

The schematic spin configurations and the decaying LR interactions of $J(r) = 1/r^{\alpha}$ for both cases are shown in Figs. 1(a)–1(c). Here we set $J = 1$ and simulate the system sizes up to $L = 64$, the inverse temperature $\beta = L/2$, and the decay exponent α from 1.5 to 100, with the focus on $\alpha \leqslant 6$. We note that to probe the ground-state properties in finite space-time size QMC simulations, one usually scales $\beta \sim L^z$, where z represents the dynamical exponents. In our problem, z is the largest at the short-ranged cases (for example, $z = 1$ for the short-range antiferromagnetic case), and our results are well converged. Since the long-range cases will only have smaller z, $\beta = L/2$ is more than sufficient to extract the ground-state properties therein. Detailed implementation and finite-size analysis of the obtained dispersions in QMC are shown in Sec. II of the Appendix.

As discussed in Refs. [85,104], for H_{FM}, the SWT analysis accompanied by a continuum approximation concludes that for $\alpha > d + 2$ (denoted as the standard Goldstone regime) where d is the spatial dimension, the low-momentum dispersion of the LR model reduces to the short-range case with $\omega \sim |\mathbf{q}|^2$, and for $d < \alpha < d + 2$ (denoted as the anomalous Goldstone regime) the dispersion is $\omega \sim |\mathbf{q}|^{\alpha - d}$. For $\alpha \leqslant d$ (denoted as the Higgs regime) the system becomes gapped because of the generalized Higgs mechanism [85]. As shown below, our QMC results are consistent with this picture as we reveal three different regimes via fitting $\omega \sim |\mathbf{q}|^{s(\alpha)}$ and finite-size analysis. When α is large, the system is in the standard Goldstone region with dispersion $\omega \sim |\mathbf{q}|^2$. As α decreases, LR interaction brings the system into the anomalous

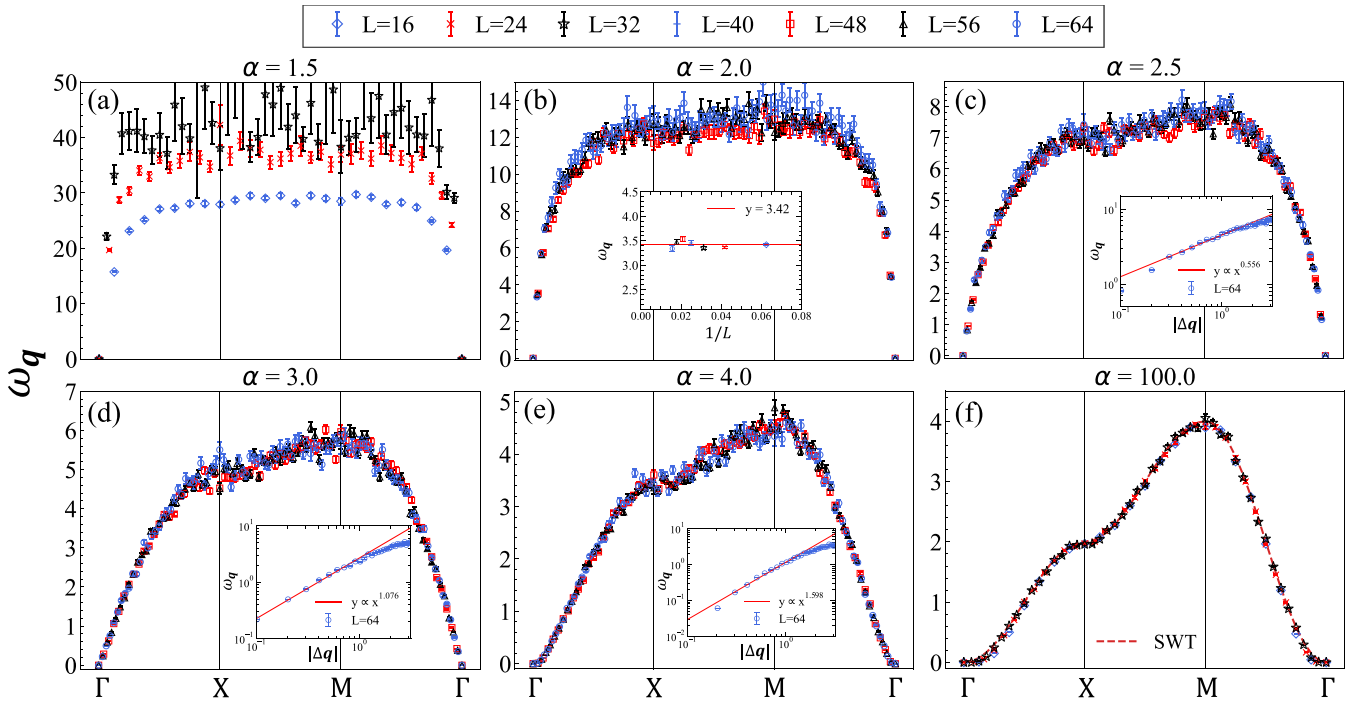

FIG. 2. Dynamical properties of 2D LR ferromagnetic Heisenberg model. Dispersion relations along the path ($\Gamma \to X \to M \to \Gamma$) with panels (a)–(f) for different decay exponents α. Results of various sizes L are plotted together in each panel and share the same legend on the top. Inset of panel (b) indicates that at $\alpha = 2$ the first excitation gaps near Γ for various sizes converge to a finite value and the system has a gaped spectrum, i.e., inside the Higgs regime. Insets of (c), (d), and (e) show the fitting of power-law dispersions $\omega_{\mathbf{q}} \sim |\mathbf{q}|^{s(\alpha)}$ near Γ (with $|\Delta\mathbf{q}|$ denotes the relative momentum away from Γ) in the range $2 < \alpha \leqslant 4$. Red dashed line in (f) is the SWT dispersion for 2D nearest-neighbor FM Heisenberg model with $\omega_{\mathbf{q}} = |J|zS(1-\gamma_{\mathbf{q}})$, where $S = 1/2$, the coordination number $z = 4$, and $\gamma_{\mathbf{q}} = \frac{1}{z}\sum_{\delta} e^{i\mathbf{q}\delta}$.

Goldstone regime, and we find exactly the same Higgs regime as in Ref. [85], which is $\alpha \leqslant 2$ [see Fig. 1(d)].

As for the antiferromagnetic case, it is worth noting that Ref. [85] predicts the Higgs regime occurs at $\alpha \leqslant d-2$ for the Hamiltonian $H = J\sum_{i\neq j}\frac{1}{|\mathbf{r}_i-\mathbf{r}_j|^{\alpha}}\mathbf{S}_i\cdot\mathbf{S}_j$. Therefore for $d = 2$ there will be no finite α values with gapped spectra, and the anomalous and standard Goldstone regimes are $d-2 < \alpha < d$ and $\alpha > d$, respectively. However, we consider a sign-problem-free Hamiltonian of Eq. (2) which does not host frustrations, and we get different boundaries of the three regimes. The system returns to the standard Goldstone mode when α is large enough, and our QMC results show the anomalous Goldstone regime is $\alpha > 2.2$ and the Higgs regime is $\alpha \leqslant 2.2$ [see Fig. 1(e)].

It is interesting to see both H_{FM} and H_{AFM} are superextensive when $\alpha \leqslant 2$, and it can be seen from Fig. 2(a) that the gap diverges with system sizes at $\alpha = 1.5$ in the ferromagnetic case. However, for H_{AFM}, the gap opens at a noninteger value $\alpha = 2.2$ [as shown in Figs. 3(a) and 3(b)], which is far beyond the expectation of similar field theory analysis with Ref. [85]. Therefore our results go beyond the conventional wisdom for long-range systems [88,99–101] and suggest the existing theory for the antiferromagnetic model needs to be modified. We further considered the Kac construction which couples a normalization factor $(N-1)/\sum_{i\neq j}\frac{1}{|r_i-r_j|^{\alpha}}$ to Eq. (1) to disentangle the effect of the superextensive nature of the Hamiltonian with the gapped spectra and perform SWT analysis on the normalized Hamiltonian. We thus confirm that the gapped spectra exist even when H_{FM} and H_{AFM} are normalized to be extensive. SWT data are presented in the Appendix.

III. RESULTS

Figure 2 shows the obtained QMC spectra along the high-symmetry path $\Gamma(0,0) \to X(\pi,0) \to M(\pi,\pi) \to \Gamma(0,0)$ for the ferromagnetic case. At $\alpha = 100$ (panel (f)), the system reduces to the short-ranged case with only nearest-neighbor couplings [10–12], and our QMC-obtained spectra matches well with the SWT spectra. Both of them show a $\omega_{\mathbf{q}} \sim |\mathbf{q}|^2$ dispersion close to Γ, and they match well along the whole path. As α gets smaller, as shown in panels (c), (d), and (e), we find the dispersion enters the anomalous Goldstone region [85], i.e., the dispersion close to Γ deviates from a quadratic one. We use $\omega_{\mathbf{q}} \sim |\mathbf{q}|^{s(\alpha)}$ to fit the dispersion close to Γ and find the power $s(\alpha)$ gradually decreases as α gets smaller. Insets of these three panels demonstrate the power-law fitting of $s(\alpha)$ using $L = 64$ QMC data. We find, at $\alpha = 3$ [panel (d)], $s = 1.076$, which agrees well with the relation of $s(\alpha) = \alpha - 2$ suggested in Ref. [85]. However, for $\alpha = 4$ [panel (e)] and $\alpha = 2.5$ [panel c)] our results show apparent derivations from $s(\alpha) = \alpha - 2$. Figure 1(d) collects the fitted power $s(\alpha)$ by QMC (red dots) at various α, and we observe a satisfactory match with our SWT results. At $\alpha = 2$ we find that $\omega_{\mathbf{q}}$ near Γ, i.e., $\mathbf{q} = (\frac{2\pi}{L}, 0)$, for different system sizes converges to a large and finite value of $\omega \approx 3.42$, as indicated in the inset of Fig. 2(b). This phenomenon is fundamentally

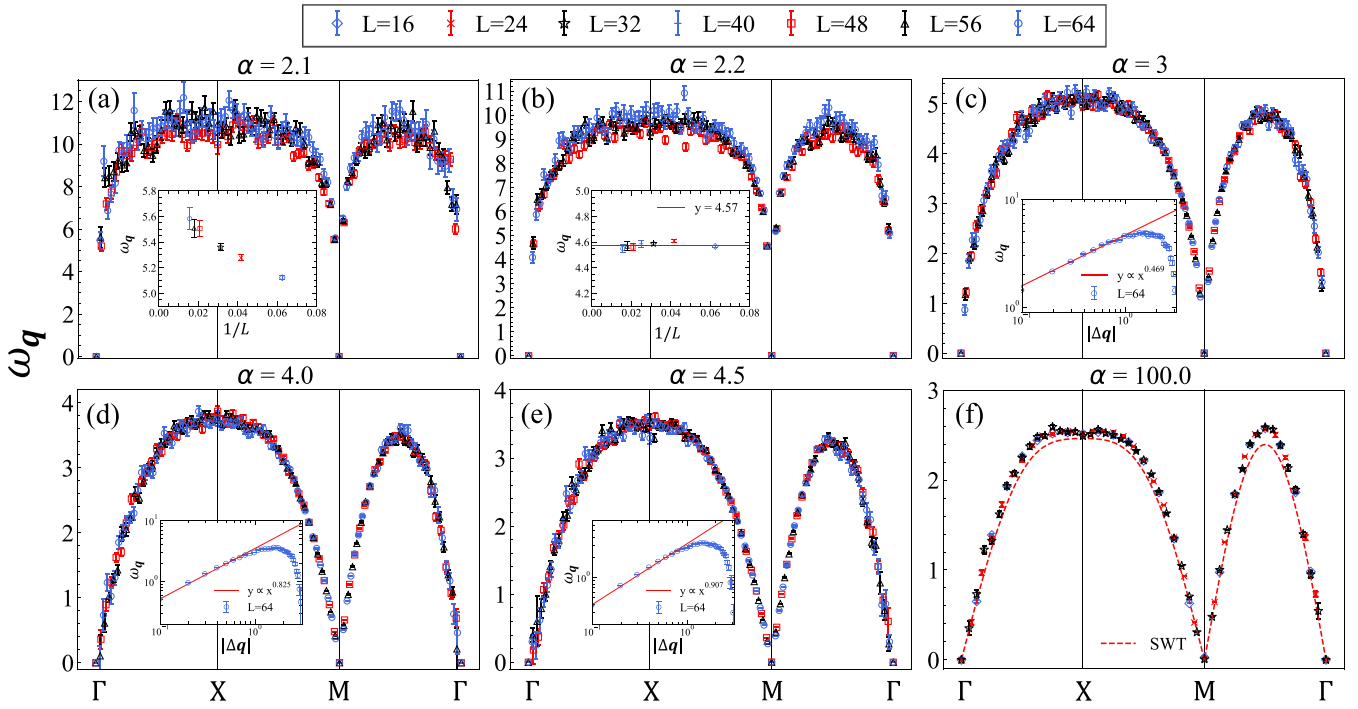

FIG. 3. Dynamical properties of 2D LR (staggered) antiferromagnetic Heisenberg model. Dispersion relations along the path ($\Gamma \to X \to M \to \Gamma$) with panels (a)–(f) for different decay exponents α. Results of various sizes L are plotted together in each panel and share the same legend on the top. Insets of panel (a) and (b) indicate that the first excitation gaps near $M = (\pi, \pi)$ for various sizes do not converge to zero (a finite value at $\alpha = 2.2$) and thus the system is inside the Higgs regime at $\alpha \leqslant 2.2$. Insets of (c), (d), and (e) show the fitting of power-law dispersion as $\omega \sim |\mathbf{q}|^{s(\alpha)}$ near M (with $|\Delta\mathbf{q}|$ denotes the relative momentum away from M) in the range $2.2 < \alpha < 4.5$. Dashed red line in (f) is the nearest-neighbor SWT dispersion $\omega_{\mathbf{q}} = |J|zS\sqrt{(1-\gamma_{\mathbf{q}})^2}$ with an additional coefficient ~1.158 to approximate the second-order spin-wave effects [76,96–98].

different from a gapless excitation in which the finite-size gap $\omega_{(2\pi/L,0)}$ converges to zero as $L \to \infty$ and results in a continuous spectra. Our result reveals that at $\alpha = 2$ the system enters the Higgs regime where the Goldstone mode acquires mass due to the LR interaction and the excitation spectrum becomes gapped. For $\alpha < 2$ [$\alpha = 1.5$ in panel (a)] we find the gaps begin to diverge with the system size L due to the aforementioned superextensive Hamiltonian. Therefore we conclude that $\alpha = 2$ is the separation power between the Higgs-type and Goldstone-type spectra in H_{FM} from our QMC results.

Figure 3 illustrates the QMC dispersion relation for H_{AFM} along the high-symmetry path. Similarly, in panel (f) we benchmark the spectrum at $\alpha = 100$ with SWT result for the short-range antiferromagnetic Hamiltonian (with an extra coefficient ~1.158 multiplied to approximate the second-order spin-wave effects [76,96–98]) and find QMC results agree well with SWT dispersion close to M with $\omega_{\mathbf{q}} \sim |\mathbf{q}|$. As α decreases, the system also enters the anomalous Goldstone region with $\omega_{\mathbf{q}} \sim |\mathbf{q}|^{s(\alpha)}$ and $0 < s(\alpha) < 1$ close to M. Fitted powers via QMC at various α are displayed in Fig. 1(e) and agree well with the SWT results. In Fig. 3(b) at $\alpha = 2.2$, $\omega_{\mathbf{q}}$ close to M converges to a large and finite value of $\omega = 4.57$. This means H_{AFM} is in the Higgs regime with gapped spectra when $\alpha \leqslant 2.2$. In fact, the inset of panel (a) for $\alpha = 2.1$ clearly forecasts a nonvanishing gap close to M at the thermodynamic limit. The inset of panel (a) seems to suggest a divergent gap at $\alpha = 2.1$; however, this may be attributed to the strong finite-size effects here. Interestingly, performing similar analysis as done in Ref. [85], one would obtain the same Higgs boundary as in the ferromagnetic case, i.e., $\alpha = 2$, which deviates from the boundary at $\alpha = 2.2$ obtained from unbiased QMC simulations. The deviation seems to suggest that antiferromagnetic quantum fluctuation plays a non-negligible role in this gap-generating process and makes it different from the ferromagnetic case. Therefore it is of interest to conduct further theoretical analysis for Eq. (2) to understand this discrepancy and reveal the subtle working of the disentanglement of the gapped spectrum and the superextensive nature of the Hamiltonian.

IV. DISCUSSION

With the unbiased large-scale QMC simulations and SWT analysis, we systematically investigate the dynamical properties of the 2D spin-1/2 Heisenberg model with LR interactions. We find that in contrast to the well-accepted low-energy customs such as Hohenberg-Mermin-Wagner theorem and gapless Goldstone mode, the LR quantum many-body systems offers richer tunability and exhibits new phenomena. As the interaction exponent α varies, the Goldstone modes can be strongly modified in that they can be either distorted (in the anomalous Goldstone regime) or even gapped via a generalized Higgs mechanism. We also find an explicit case where the gapped excitation exists even when the Hamiltonian is extensive.

These dynamical properties have immediate relevance to the ongoing experiments with ultracold atom arrays and quantum moiré materials. For example, the long-range Coulomb interaction in quantum moiré systems can be easily tuned by varying dielectric environment, electrostatic gating, and twisting angles, and in this way observed thermodynamic and dynamical properties (such as switching between gapped and gapless spectra) [34,59,60,65,66,68] can be identified with different LR interaction types and regimes when compared unbiased results such as ours. Similar tunability can also be realized in dressed Rydberg atom arrays whose interaction can be modified [105]. One can then compare different responses from experiments with our results to identify the LR interaction and the novel phases.

ACKNOWLEDGMENTS

We thank Zheng Yan, Tianyu Wu, Ting-Tung Wang, Yuan Da Liao, Qi Yang, Meng Cheng, and Fakher Assaad for valuable discussions on related topics. We acknowledge support from the Research Grants Council of Hong Kong SAR of China (Projects No. 17301420, No. 17301721, No. AoE/P-701/20, No. 17309822, No. HKU C7037-22G), the ANR/RGC Joint Research Scheme sponsored by Research Grants Council of Hong Kong SAR of China and the French National Research Agency (Project No. A_HKU703/22), the K. C. Wong Education Foundation (Grant No. GJTD-2020-01), and the Seed Funding Quantum-Inspired explainable-AI at the HKU-TCL Joint Research Centre for Artificial Intelligence. We thank the HPC2021 system under the Information Technology Services and the Blackbody HPC system at the Department of Physics, the University of Hong Kong for their technical support and generous allocation of CPU time. The authors also acknowledge the National Supercomputer Centers in Guangzhou, the Beijng PARATERA Tech CO., Ltd., for providing HPC resources that have contributed to the research results reported within this paper.

APPENDIX

In this Appendix we present the linear spin-wave analysis for the LR FM and staggered AFM Heisenberg model in which the dispersion relation of the low-lying magnetic excitations at different decaying power α are extracted. From here we make comparisons with the dispersion obtained from the QMC simulations in the main text. Spin-wave analysis with Kac construction is presented. Moreover, we outline the QMC procedure and provide detailed data on the fitting of the excitation gaps from the dynamical correlation functions obtained in QMC simulations.

1. Linear spin-wave analysis

We applied the linear spin-wave theory (SWT) to analyze the dispersion of the low-energy excitation in the LR spin-1/2 Heisenberg model with power-law decaying couplings in both ferromagnetic and staggered antiferromagnetic cases [12,94–98]. Taking the staggered antiferromagnetic cases as an example, it calls for the definition of two sublattices, A and B. The spin on each sublattice is pointing in the same direction. Then we rewrite the spin operators by $S^+ = S^x + iS^y$ and $S^- = S^x - iS^y$ and apply the Holstein-Primakoff transformation up to order S that for sublattice A,

$$\begin{aligned} S_i^z &= S - a_i^\dagger a_i, \\ S_i^+ &= \sqrt{2S} a_i, \\ S_i^- &= \sqrt{2S} a_i^\dagger, \end{aligned} \tag{A1}$$

and for sublattice B,

$$\begin{aligned} S_i^z &= b_i^\dagger b_i - S, \\ S_i^+ &= \sqrt{2S} b_i^\dagger, \\ S_i^- &= \sqrt{2S} b_i. \end{aligned} \tag{A2}$$

Here we take $S = 1/2$ and the Hamiltonian in the momentum space is given by

$$\begin{aligned} H_{sw} &= \sum_{\mathbf{q}} \gamma^\dagger(\mathbf{q}) H_{\mathbf{q}} \gamma(\mathbf{q}), \\ H_{\mathbf{q}} &= \begin{bmatrix} J_0^d + J_0^s - J_{\mathbf{q}}^s & J_{\mathbf{q}}^d \\ J_{\mathbf{q}}^d & J_0^d + J_0^s - J_{\mathbf{q}}^s \end{bmatrix}, \end{aligned} \tag{A3}$$

in which $\gamma^\dagger(\mathbf{q}) = (a_{\mathbf{q}}^\dagger, b_{\mathbf{q}})$ and $a_{\mathbf{q}}^\dagger$ is Fourier transformed so that $a_{\mathbf{q}}^\dagger = N^{1/2} \sum_{\mathbf{r}} a_i^\dagger e^{-i\mathbf{q}\mathbf{r}}$. Here $J_{\mathbf{q}}^s = \sum_{\mathbf{r}^s \in \text{same}} e^{-i\mathbf{q}\mathbf{r}^s} J_{\mathbf{r}}^s$ refers to the coupling between the spins belonging to the same sublattice, and $J_{\mathbf{q}}^d = \sum_{\mathbf{r}^d \in \text{diff}} e^{-i\mathbf{q}\mathbf{r}^d} J_{\mathbf{r}}^d$ to that of the different sublattices. $J_{\mathbf{r}}^{d(s)} = 1/|\Delta r|^\alpha$ is the coupling strength. Finally, the single-magnon dispersion relation of the LR Heisenberg model with staggered antiferromagnetic power-law decaying couplings is given by

$$\omega_{\mathbf{q}}^{\text{AFM}} = \sqrt{\left(J_0^d + J_0^s - J_{\mathbf{q}}^s + J_{\mathbf{q}}^d\right)\left(J_0^d + J_0^s - J_{\mathbf{q}}^s - J_{\mathbf{q}}^d\right)}. \tag{A4}$$

Similarly, in the ferromagnetic case the dispersion relation of the single magnon can be read as $\omega_{\mathbf{q}}^{\text{FM}} = |J_0 - J_{\mathbf{q}}|$ with $J_{\mathbf{q}} = \sum_{\mathbf{r}} e^{-i\mathbf{q}\mathbf{r}} J_{\mathbf{r}}$.

To capture the dependence of the dispersion relation to α in Eqs. (1) and (2) in the main text, we numerically calculate the linear SWT results by applying a cutoff of longest range coupling as $r_{\max}$, meaning that we only consider the coupling between the sites (r_x, r_y) and $(r_x + \Delta r_x, r_y + \Delta r_y)$ with Δr_x and Δr_y ranging from $-r_{\max}/2$ to $r_{\max}/2$, and we have computed $r_{\max}$ up to 1000.

Figure 4(a) describes the dispersion relation of the linear SWT along the momentum path $\Gamma \to X \to M \to \Gamma$ with α changing from $\alpha = 2.0$ to 4.0. For large α, the LR coupling rapidly decays, which makes its dispersion relation of single magnon similar to that of the typical antiferromagnetic square lattice only with nearest-neighbor coupling. Here the single-magnon dispersion relation is gapless only at Γ and M. As α decreases, the LR couplings strongly distort the dispersion relation, which makes the magnon excitation cost more energy and the dispersion relation goes higher as α decreases. But this dispersion relation obtained from the linear SWT theory still remains gapless at Γ and M. Actually, the single-magnon dispersion relation would become discrete at Γ and M in the limit $r_{\max} \to \infty$.

With $\Delta\mathbf{q}$ the relative momentum away from the M point, we plot the dispersion relation along the $M \to \Gamma$ direction

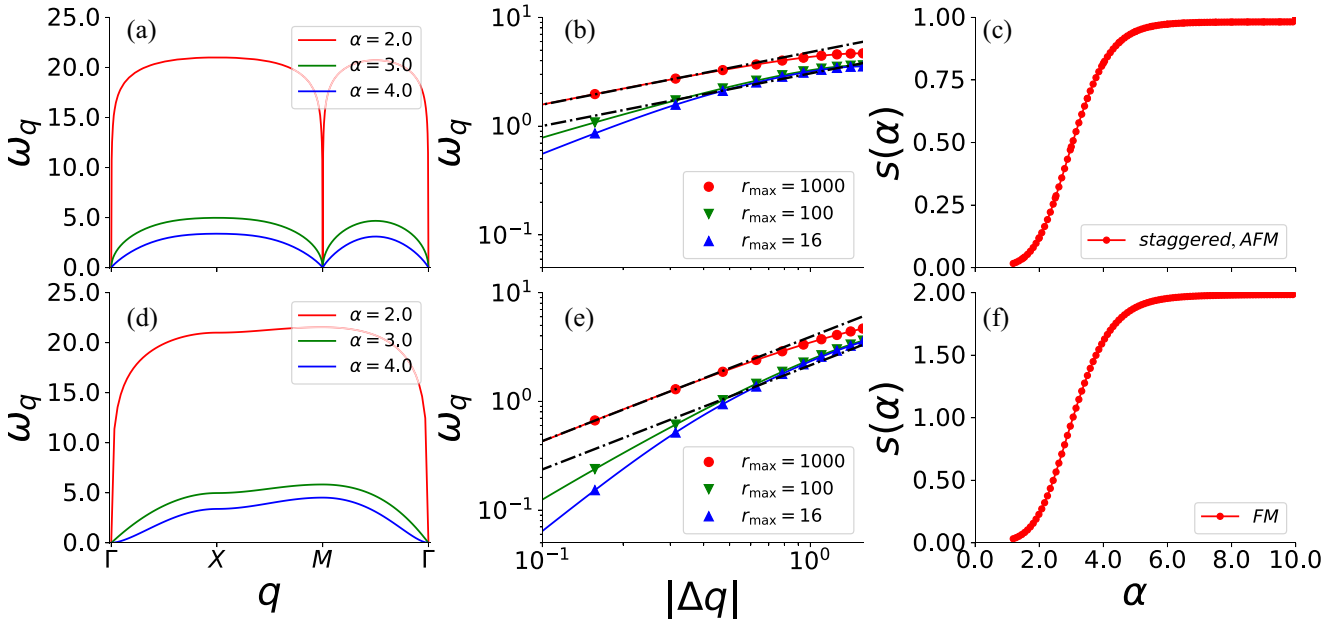

FIG. 4. The linear SWT results. Panels (a), (b), and (c) are the linear spin-wave result of the staggered antiferromagnetic case, while (d), (e), and (f) are the ferromagnetic case. Panels (a) and (d) are the dispersion relation plotted along the momentum path $\Gamma \to X \to M \to \Gamma$ with $r_{\max} = 1000$. (b) The spin-wave dispersion relation near the M point for the staggered antiferromagnetic lattice with $\alpha = 3.5$ and $r_{\max}$ ranges from 16 to 1000, while (e) shows the Γ point in the ferromagnetic case. The two black dashed lines here refer to the relation $\omega_{\mathbf{q}} \propto |\Delta\mathbf{q}|^{0.48}$ in (b), and $\omega_{\mathbf{q}} \propto |\Delta\mathbf{q}|^{0.96}$ in (e). (c), and (f) describe the relation between the power of the dispersion $s(\alpha)$ as a function of decay exponent α, obtained from fittings with $r_{\max} = 1000$.

in Fig. 4(b) with a double-logarithmic scale at $\alpha = 3.5$ with varying $r_{\max}$, which shows the power-law dependence between $\Delta\mathbf{q}$ and ω. We fit the linear SWT results with $\omega_{\mathbf{q}} = A|\Delta\mathbf{q}|^s$ near the M point. Note that for small $r_{\max}$ ($r_{\max} \leqslant 100$), the single-magnon dispersion around the M point still depends on $r_{\max}$, which is shown in Fig. 4(b) with $r_{\max}$ changing from 16 to 1000. Such a dependence would disappear and s would finally converge in the limit $r_{\max} \to \infty$. In order to demonstrate this convergence process as $r_{\max} \to \infty$, we plot two black dashed lines that $\omega_{\mathbf{q}} \propto |\Delta\mathbf{q}|^{0.48}$ in (b), where $s = 0.48$ comes from the fitting of the linear SWT result with $r_{\max} = 1000$. In Fig. 4(b), as $r_{\max}$ increases, s converges to 0.48. Finally, with $r_{\max} = 1000$, Fig. 4(c) presents our fitting about the relation between the power $s(\alpha)$ and the decay exponent α, which suggests the limit $r_{\max} \to \infty$ and is also plotted as the blue dots in Fig. 1(d) in the main text.

Similarly, we also plot our linear SWT results of the ferromagnetic case in Figs. 4(d), 4(e) and 4(f). Figure 4(f) also shows the relation between the power $s(\alpha)$ and α taking $r_{\max} = 1000$, which is also given as the blue dots in Fig. 1(e) in the main text.

In addition, the Hamiltonian Eqs. (1) and (2) are superextensive for $\alpha \leqslant 2$, and their ground-state energy diverges superlinearly with the number of sites N. Historically, to suppresses such a divergence of the ground-state energy, the Kac construction has been proposed [88,99–101]. By coupling a normalization factor $\mathcal{N}$ to the Hamiltonian, Eqs. (1) and (2) become

$$H_{\mathrm{FM}}^{Kac} = -\mathcal{N}J \sum_{i \neq j} \frac{1}{|\mathbf{r}_i - \mathbf{r}_j|^{\alpha}} \mathbf{S}_i \cdot \mathbf{S}_j, \tag{A5}$$

$$H_{\mathrm{AFM}}^{Kac} = \mathcal{N}J \sum_{i \neq j} \frac{(-1)^{|x_i+y_i-x_j-y_j+1|}}{|\mathbf{r}_i - \mathbf{r}_j|^{\alpha}} \mathbf{S}_i \cdot \mathbf{S}_j, \tag{A6}$$

$$\mathcal{N} = \frac{N-1}{\sum_{i \neq j} \frac{1}{|r_i - r_j|^{\alpha}}}. \tag{A7}$$

Here $\sum_{i \neq j}$ means a sum over all $i \neq j$. For convenience of linear SWT analysis, we rewrite $\mathcal{N}$ by

$$\mathcal{N} = \frac{N-1}{N} \frac{1}{\sum_{j \neq i_0} \frac{1}{2|r_{i_0} - r_j|^{\alpha}}}. \tag{A8}$$

Since $\lim_{N \to \infty} \frac{N-1}{N} = 1$, Eq. (A8) actually introduces a factor $1/[\sum_j \frac{1}{2|r_{i_0} - r_j|^{\alpha}}]$ to the Hamiltonian of the linear SWT in the momentum space [like Eq. (A3)].

To see whether the normalization factor Eq. (A7) influences the excitation gap in the Higgs regime, we calculate the spin-wave dispersion $\omega(\Delta\mathbf{q} = 2\pi/r_{\max})$ at the momentum point $\Gamma + \Delta\mathbf{q}$ for the ferromagnetic case ($M + \Delta\mathbf{q}$ for the antiferromagnetic case) with $r_{\max} \to \infty$, which is plotted in Fig. 5. Figure 5(a) stands for the staggered antiferromagnetic coupling, while (b) is for the ferromagnetic case. α ranges from 1.5 to 1.7 in both cases. As it is shown, for both cases, $\omega(2\pi/r_{\max})$ converges to a finite constant as $r_{\max} \to \infty$, even with the normalization factor from Kac construction. Such a behavior proves the spectra in the Higgs regime remain

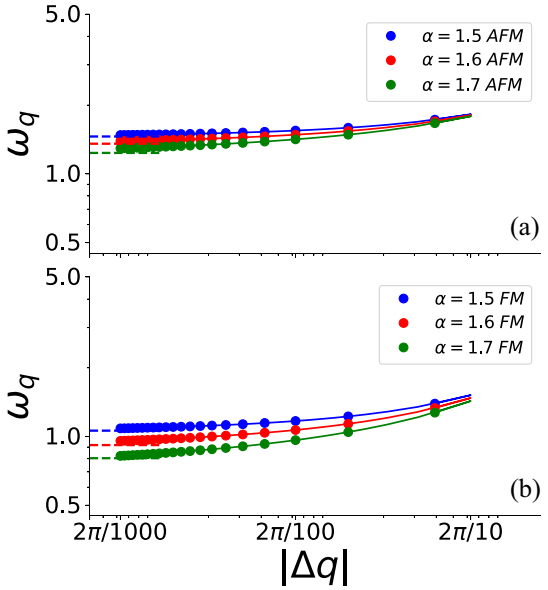

FIG. 5. The linear SWT results considering the Kac normalization. Panel (a) is for the staggered antiferromagnetic coupling and describes the spin-wave dispersion relation near the M point, while (b) stands for the ferromagnetic case and near the Γ point. $|\Delta\mathbf{q}| = 2\pi/r_{\max}$, with $r_{\max}$ ranging from 16 to 1000. The blue, green, and red lines refer to $\alpha = 1.5,\ 1.6,\ 1.7$. The dashed line is the energy gap Δ observed by fitting $\omega(\Delta\mathbf{q})$ with $a|\mathbf{q}|^b + \Delta$.

gapped even with the Kac construction, and our conclusion is not affected by the divergence of the ground-state energy.

2. Fitting with QMC data

In order to obtain the low-energy spectra of $H_{\rm FM}$ and $H_{\rm AFM}$ in QMC [26,83,92,93], we compute the imaginary time correlation function $G_{\mathbf{q}}(\tau) \equiv \langle S^z_{\mathbf{q}}(\tau) S^z_{-\mathbf{q}}(0)\rangle - \langle S^z_{\mathbf{q}}\rangle^2$, where $S^z_{\mathbf{q}} \equiv \frac{1}{\sqrt{N}} \sum_{\mathbf{r}} e^{i\mathbf{q}\cdot\mathbf{r}} S^z_{\mathbf{r}}$. Here we consider the periodic boundary conditions in the simulation so that $(q_x, q_y) = (\pm\frac{2\pi m}{L}, \pm\frac{2\pi n}{L})$, with m and n being integers that are physical momenta on a $L \times L$ square lattice. The loop update scheme of SSE QMC is purposely adapted to cope with the long-range interactions

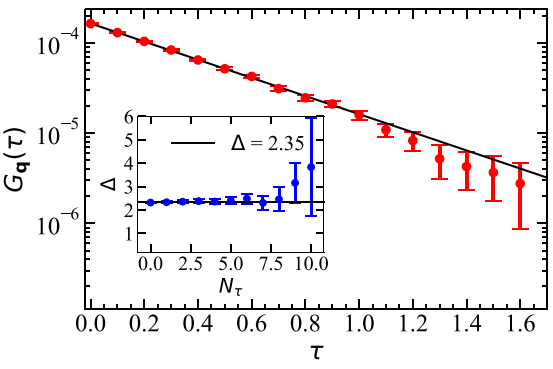

FIG. 6. The fitting of energy gap with the data of the correlation function $G_{\mathbf{q}}(\tau)$ vs τ for $L = 64$ and $\alpha = 2.5$ at $\mathbf{q} = (3 \times 2\pi/L, 0)$ for the ferromagnetic case. The inset shows the obtained gap when the first N_τ data points are omitted before fitting.

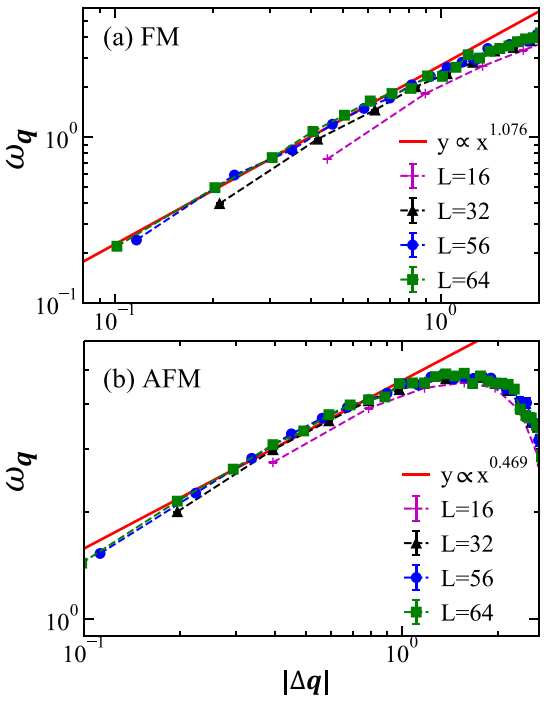

FIG. 7. Dispersion relation at $\alpha = 3$ for various system sizes L. (a) Dispersion of $H_{\rm FM}$ near Γ with $\Delta\mathbf{q}$ denotes the relative momentum away from Γ. Red line $y \propto x^{1.076}$ shows the fitted power $s(\alpha = 3) = 1.076$ using $L = 64$ QMC data. (b) Dispersion of $H_{\rm AFM}$ near M with $\Delta\mathbf{q}$ denotes the relative momentum away from M. Red line $y \propto x^{0.469}$ shows the fitted power $s(\alpha = 3) = 0.469$ using $L = 64$ QMC data.

by assigning each bond with a separate bond weight and bond type (ferromagnetic or antiferromagnetic) [106]:

$$\left\langle S^z_{\mathbf{q}}(\tau) S^z_{-\mathbf{q}}(0)\right\rangle = \left\langle e^{H\tau} S^z_{\mathbf{q}}(0) e^{-H\tau} S^z_{-\mathbf{q}}(0)\right\rangle = \left(\sum_{l=0}^{\infty} e^{-\beta E_l}\right)^{-1} \times \sum_{n,m=0}^{\infty} \left|\langle n|S^z_{\mathbf{q}}|m\rangle\right|^2 e^{-(E_m - E_n)\tau} e^{-\beta E_n} \quad \text{(A9)}$$

where $H|n\rangle = E_n|n\rangle$ and E_0 is the ground-state energy of the system. When $\beta\Delta E_1 \gg 1$ where $\Delta E_n = E_n - E_0$, we can estimate

$$G_{\mathbf{q}}(\tau) \approx \sum_{n=1}^{\infty} \left|\langle 0|S^z_{\mathbf{q}}|n\rangle\right|^2 (e^{-\Delta E_n(\mathbf{q})\tau} + e^{-\Delta E_n(\mathbf{q})(\beta-\tau)}). \quad \text{(A10)}$$

When the imaginary time τ is sufficiently large, we assume that the system will gradually evolve to the ground state and only the slowing decaying exponential term exists, so that the correlation function can be further approximated by

$$G_{\mathbf{q}}(\tau) \approx \left|\langle 0|S^z_{\mathbf{q}}|1\rangle\right|^2 e^{-\Delta E_1(\mathbf{q})\tau}. \quad \text{(A11)}$$

If $|\langle 0|S^z_{\mathbf{q}}|1\rangle|^2$ is finite (which is usually the case), we can then extract the energy gap for each $\mathbf{q}$ point by fitting $G_{\mathbf{q}}(\tau)$ with an exponentially decaying function.

We fit the QMC data of $G_{\mathbf{q}}(\tau)$ by the relation $G_{\mathbf{q}}(\tau) \propto e^{-\Delta_{\mathbf{q}}\tau}$, and the fitting process is shown in Fig. 6. We first choose the data points for fitting according to their relative

errors. If the relative error of one data point is less than 0.2, then the data point is chosen to be used for fitting. In the fitting process, we gradually omit the first N_τ data points and then do the curve fitting to find the most probable gap. As shown in the inset of Fig. 6, the fitting error becomes intolerant when $N_\tau = 10$, and the fitted gap converges around $\Delta = 2.35$ when N_τ gradually decreases to 0. In this case we choose $\Delta = 2.35$ to be the fitted gap for the data. Note that we find that for all the $\mathbf{q}$ points at different α, the fitted gap does not change evidently with N_τ, which means that higher excited states have much bigger energy gaps than the first excited states ($\Delta E_2 \gg \Delta E_1$) so that the $e^{-\Delta E_1 \tau}$ term in $G_{\mathbf{q}}(\tau)$ contributes much more than the other terms for the range of τ we consider.

Figure 7(a) shows the dispersion of H_{FM} near Γ, and Fig. 7(b) shows the dispersion of H_{AFM} near M for various system sizes L at $\alpha = 3$. $|\Delta\mathbf{q}|$ denotes the relative momentum away from the Γ in (a) [M in (b)]. Plotting under a double logarithm scale, it is demonstrated that the power of low-momentum dispersion $s(\alpha)$ depends on the system size L. However, as the system size L increases, the dispersion gradually converges and $s(\alpha)$ will finally remain unchanged as $L \to \infty$. Such a process can already be seen, as the vast majority of $L = 56$ and $L = 64$ data collapse onto the same curve in both FM and AFM cases. We thus obtain $s(\alpha)$ by fitting $L = 64$ data, and $y \propto x^{s(\alpha)}$ is plotted as red lines in Fig. 7. The same red lines are shown in the insets (c), (d), and (e) in Figs. 2 and 3 in the main text.

[1] P. C. Hohenberg, Existence of long-range order in one and two dimensions, Phys. Rev. **158**, 383 (1967).

[2] N. D. Mermin and H. Wagner, Absence of Ferromagnetism or Antiferromagnetism in One- or Two-Dimensional Isotropic Heisenberg Models, Phys. Rev. Lett. **17**, 1133 (1966).

[3] M. Weber, D. J. Luitz, and F. F. Assaad, Dissipation-Induced Order: The $s = 1/2$ Quantum Spin Chain Coupled to an Ohmic Bath, Phys. Rev. Lett. **129**, 056402 (2022).

[4] Z. Wang, F. Assaad, and M. Ulybyshev, Validity of SLAC fermions for the $(1 + 1)$-dimensional helical Luttinger liquid, Phys. Rev. B **108**, 045105 (2023).

[5] P. Werner, M. Troyer, and S. Sachdev, Quantum spin chains with site dissipation, J. Phys. Soc. Jpn. **74**, 67 (2005).

[6] Y. Da Liao, X. Y. Xu, Z. Y. Meng, and Y. Qi, Caution on Gross-Neveu criticality with a single Dirac cone: Violation of locality and its consequence of unexpected finite-temperature transition, arXiv:2210.04272.

[7] B. I. Halperin, On the Hohenberg-Mermin-Wagner theorem and its limitations, J. Stat. Phys. **175**, 521 (2019).

[8] Z. Li, S. Choudhury, and W. V. Liu, Long-range-ordered phase in a quantum Heisenberg chain with interactions beyond nearest neighbors, Phys. Rev. A **104**, 013303 (2021).

[9] D. Peter, S. Müller, S. Wessel, and H. P. Büchler, Anomalous Behavior of Spin Systems with Dipolar Interactions, Phys. Rev. Lett. **109**, 025303 (2012).

[10] M. E. Fisher, S.-k. Ma, and B. G. Nickel, Critical Exponents for Long-Range Interactions, Phys. Rev. Lett. **29**, 917 (1972).

[11] J. Sak, Recursion relations and fixed points for ferromagnets with long-range interactions, Phys. Rev. B **8**, 281 (1973).

[12] N. Defenu, T. Donner, T. Macrì, G. Pagano, S. Ruffo, and A. Trombettoni, Long-range interacting quantum systems, arXiv:2109.01063.

[13] J. A. Koziol, A. Langheld, S. C. Kapfer, and K. P. Schmidt, Quantum-critical properties of the long-range transverse-field Ising model from quantum Monte Carlo simulations, Phys. Rev. B **103**, 245135 (2021).

[14] S. Fey, S. C. Kapfer, and K. P. Schmidt, Quantum Criticality of Two-Dimensional Quantum Magnets with Long-Range Interactions, Phys. Rev. Lett. **122**, 017203 (2019).

[15] P. Adelhardt and K. P. Schmidt, Continuously varying critical exponents in long-range quantum spin ladders, arXiv:2209.01182.

[16] T. Koffel, M. Lewenstein, and L. Tagliacozzo, Entanglement Entropy for the Long-Range Ising Chain in a Transverse Field, Phys. Rev. Lett. **109**, 267203 (2012).

[17] W. Jiang, B.-B. Chen, Z. H. Liu, J. Rong, F. F. Assaad, M. Cheng, K. Sun, and Z. Y. Meng, Fermion disorder operator: The hedgehog and the fox of quantum many-body entanglement, arXiv:2209.07103.

[18] J. Zhao, Y.-C. Wang, Z. Yan, M. Cheng, and Z. Y. Meng, Scaling of Entanglement Entropy at Deconfined Quantum Criticality, Phys. Rev. Lett. **128**, 010601 (2022).

[19] Y.-C. Wang, N. Ma, M. Cheng, and Z. Y. Meng, Scaling of the disorder operator at deconfined quantum criticality, SciPost Phys. **13**, 123 (2022).

[20] Z. H. Liu, W. Jiang, B.-B. Chen, J. Rong, M. Cheng, K. Sun, Z. Y. Meng, and F. F. Assaad, Fermion Disorder Operator at Gross-Neveu and Deconfined Quantum Criticalities, Phys. Rev. Lett. **130**, 266501 (2023).

[21] Y. Da Liao, G. Pan, W. Jiang, Y. Qi, and Z. Y. Meng, The teaching from entanglement: 2D deconfined quantum critical points are not conformal, arXiv:2302.11742.

[22] R. Samajdar, W. W. Ho, H. Pichler, M. D. Lukin, and S. Sachdev, Quantum phases of Rydberg atoms on a kagome lattice, Proc. Natl. Acad. Sci. USA **118**, e2015785118 (2021).

[23] Z. Yan, R. Samajdar, Y.-C. Wang, S. Sachedev, and Z. Y. Meng, Triangular lattice quantum dimer model with variable dimer density, Nat. Commun. **13**, 5799 (2022).

[24] G. Semeghini, H. Levine, A. Keesling, S. Ebadi, T. T. Wang, D. Bluvstein, R. Verresen, H. Pichler, M. Kalinowski, R. Samajdar, A. Omran, S. Sachdev, A. Vishwanath, M. Greiner, V. Vuletić, and M. D. Lukin, Probing topological spin liquids on a programmable quantum simulator, Science **374**, 1242 (2021).

[25] K. J. Satzinger, Y. J. Liu, A. Smith, C. Knapp, M. Newman, C. Jones, Z. Chen, C. Quintana, X. Mi, A. Dunsworth, C. Gidney, I. Aleiner, F. Arute, K. Arya, J. Atalaya, R. Babbush, J. C. Bardin, R. Barends, J. Basso, A. Bengtsson *et al.*, Realizing topologically ordered states on a quantum processor, Science **374**, 1237 (2021).

[26] Z. Yan, Y.-C. Wang, R. Samajdar, S. Sachdev, and Z. Y. Meng, Emergent Glassy Behavior in a Kagome Rydberg Atom Array, Phys. Rev. Lett. **130**, 206501 (2023).

[27] G. Trambly de Laissardière, D. Mayou, and L. Magaud, Localization of Dirac electrons in rotated graphene bilayers, Nano Lett. **10**, 804 (2010).

[28] R. Bistritzer and A. H. MacDonald, Moire bands in twisted double-layer graphene, Proc. Natl. Acad. Sci. USA **108**, 12233 (2011).

[29] J. M. B. Lopes dos Santos, N. M. R. Peres, and A. H. Castro Neto, Continuum model of the twisted graphene bilayer, Phys. Rev. B **86**, 155449 (2012).

[30] Y. Cao, V. Fatemi, S. Fang, K. Watanabe, T. Taniguchi, E. Kaxiras, and P. Jarillo-Herrero, Unconventional superconductivity in magic-angle graphene superlattices, Nature (London) **556**, 43 (2018).

[31] Y. Cao, V. Fatemi, A. Demir, S. Fang, S. L. Tomarken, J. Y. Luo, J. D. Sanchez-Yamagishi, K. Watanabe, T. Taniguchi, E. Kaxiras *et al.*, Correlated insulator behaviour at half-filling in magic-angle graphene superlattices, Nature (London) **556**, 80 (2018).

[32] Y. Xie, B. Lian, B. Jäck, X. Liu, C.-L. Chiu, K. Watanabe, T. Taniguchi, B. A. Bernevig, and A. Yazdani, Spectroscopic signatures of many-body correlations in magic-angle twisted bilayer graphene, Nature (London) **572**, 101 (2019).

[33] X. Lu, P. Stepanov, W. Yang, M. Xie, M. A. Aamir, I. Das, C. Urgell, K. Watanabe, T. Taniguchi, G. Zhang *et al.*, Superconductors, orbital magnets and correlated states in magic-angle bilayer graphene, Nature (London) **574**, 653 (2019).

[34] A. Kerelsky, L. J. McGilly, D. M. Kennes, L. Xian, M. Yankowitz, S. Chen, K. Watanabe, T. Taniguchi, J. Hone, C. Dean *et al.*, Maximized electron interactions at the magic angle in twisted bilayer graphene, Nature (London) **572**, 95 (2019).

[35] Y. Da Liao, Z. Y. Meng, and X. Y. Xu, Valence Bond Orders at Charge Neutrality in a Possible Two-Orbital Extended Hubbard Model for Twisted Bilayer Graphene, Phys. Rev. Lett. **123**, 157601 (2019).

[36] M. Yankowitz, S. Chen, H. Polshyn, Y. Zhang, K. Watanabe, T. Taniguchi, D. Graf, A. F. Young, and C. R. Dean, Tuning superconductivity in twisted bilayer graphene, Science **363**, 1059 (2019).

[37] S. L. Tomarken, Y. Cao, A. Demir, K. Watanabe, T. Taniguchi, P. Jarillo-Herrero, and R. C. Ashoori, Electronic Compressibility of Magic-Angle Graphene Superlattices, Phys. Rev. Lett. **123**, 046601 (2019).

[38] Y. Cao, D. Chowdhury, D. Rodan-Legrain, O. Rubies-Bigorda, K. Watanabe, T. Taniguchi, T. Senthil, and P. Jarillo-Herrero, Strange Metal in Magic-Angle Graphene with near Planckian Dissipation, Phys. Rev. Lett. **124**, 076801 (2020).

[39] C. Shen, Y. Chu, Q. Wu, N. Li, S. Wang, Y. Zhao, J. Tang, J. Liu, J. Tian, K. Watanabe, T. Taniguchi, R. Yang, Z. Y. Meng, D. Shi, O. V. Yazyev, and G. Zhang, Correlated states in twisted double bilayer graphene, Nat. Phys. **16**, 520 (2020).

[40] S. Chatterjee, M. Ippoliti, and M. P. Zaletel, Skyrmion superconductivity: DMRG evidence for a topological route to superconductivity, Phys. Rev. B **106**, 035421 (2022).

[41] E. Khalaf, N. Bultinck, A. Vishwanath, and M. P. Zaletel, Soft modes in magic angle twisted bilayer graphene, arXiv:2009.14827.

[42] M. Xie and A. H. MacDonald, Nature of the Correlated Insulator States in Twisted Bilayer Graphene, Phys. Rev. Lett. **124**, 097601 (2020).

[43] A. T. Pierce, Y. Xie, J. M. Park, E. Khalaf, S. H. Lee, Y. Cao, D. E. Parker, P. R. Forrester, S. Chen, K. Watanabe *et al.*, Unconventional sequence of correlated Chern insulators in magic-angle twisted bilayer graphene, Nat. Phys. **17**, 1210 (2021).

[44] Y.-D. Liao, X.-Y. Xu, Z.-Y. Meng, and J. Kang, Correlated insulating phases in the twisted bilayer graphene, Chin. Phys. B **30**, 017305 (2021).

[45] A. Rozen, J. M. Park, U. Zondiner, Y. Cao, D. Rodan-Legrain, T. Taniguchi, K. Watanabe, Y. Oreg, A. Stern, E. Berg *et al.*, Entropic evidence for a Pomeranchuk effect in magic-angle graphene, Nature (London) **592**, 214 (2021).

[46] U. Zondiner, A. Rozen, D. Rodan-Legrain, Y. Cao, R. Queiroz, T. Taniguchi, K. Watanabe, Y. Oreg, F. von Oppen, A. Stern *et al.*, Cascade of phase transitions and Dirac revivals in magic-angle graphene, Nature (London) **582**, 203 (2020).

[47] Y. Saito, F. Yang, J. Ge, X. Liu, T. Taniguchi, K. Watanabe, J. Li, E. Berg, and A. F. Young, Isospin Pomeranchuk effect in twisted bilayer graphene, Nature (London) **592**, 220 (2021).

[48] J. M. Park, Y. Cao, K. Watanabe, T. Taniguchi, and P. Jarillo-Herrero, Flavour Hund's coupling, Chern gaps and charge diffusivity in moiré graphene, Nature (London) **592**, 43 (2021).

[49] Y. H. Kwan, Y. Hu, S. H. Simon, and S. A. Parameswaran, Exciton Band Topology in Spontaneous Quantum Anomalous Hall Insulators: Applications to Twisted Bilayer Graphene, Phys. Rev. Lett. **126**, 137601 (2021).

[50] Y. Da Liao, J. Kang, C. N. Breiø, X. Y. Xu, H.-Q. Wu, B. M. Andersen, R. M. Fernandes, and Z. Y. Meng, Correlation-Induced Insulating Topological Phases at Charge Neutrality in Twisted Bilayer Graphene, Phys. Rev. X **11**, 011014 (2021).

[51] J. Liu and X. Dai, Theories for the correlated insulating states and quantum anomalous Hall effect phenomena in twisted bilayer graphene, Phys. Rev. B **103**, 035427 (2021).

[52] F. Schindler, O. Vafek, and B. A. Bernevig, Trions in twisted bilayer graphene, Phys. Rev. B **105**, 155135 (2022).

[53] Z.-D. Song and B. A. Bernevig, Magic-Angle Twisted Bilayer Graphene as a Topological Heavy Fermion Problem, Phys. Rev. Lett. **129**, 047601 (2022).

[54] J.-X. Lin, Y.-H. Zhang, E. Morissette, Z. Wang, S. Liu, D. Rhodes, K. Watanabe, T. Taniguchi, J. Hone, and J. Li, Spin-orbit–driven ferromagnetism at half moiré filling in magic-angle twisted bilayer graphene, Science **375**, 437 (2022).

[55] T. Huang, X. Tu, C. Shen, B. Zheng, J. Wang, H. Wang, K. Khaliji, S. H. Park, Z. Liu, T. Yang *et al.*, Observation of chiral and slow plasmons in twisted bilayer graphene, Nature (London) **605**, 63 (2022).

[56] S. Zhang, X. Lu, and J. Liu, Correlated Insulators, Density Wave States, and Their Nonlinear Optical Response in Magic-Angle Twisted Bilayer Graphene, Phys. Rev. Lett. **128**, 247402 (2022).

[57] J. Herzog-Arbeitman, A. Chew, D. K. Efetov, and B. A. Bernevig, Reentrant Correlated Insulators in Twisted Bilayer Graphene at 25 T (2π flux), Phys. Rev. Lett. **129**, 076401 (2022).

[58] E. Y. Andrei and A. H. MacDonald, Graphene bilayers with a twist, Nat. Mater. **19**, 1265 (2020).

[59] P. Stepanov, M. Xie, T. Taniguchi, K. Watanabe, X. Lu, A. H. MacDonald, B. A. Bernevig, and D. K. Efetov, Competing

Zero-Field Chern Insulators in Superconducting Twisted Bilayer Graphene, Phys. Rev. Lett. **127**, 197701 (2021).

[60] G. Pan, X. Zhang, H. Lu, H. Li, B.-B. Chen, K. Sun, and Z. Y. Meng, Thermodynamic Characteristic for a Correlated Flat-Band System with a Quantum Anomalous Hall Ground State, Phys. Rev. Lett. **130**, 016401 (2023).

[61] X. Zhang, G. Pan, Y. Zhang, J. Kang, and Z. Y. Meng, Momentum space quantum Monte Carlo on twisted bilayer graphene, Chin. Phys. Lett. **38**, 077305 (2021).

[62] J. S. Hofmann, E. Khalaf, A. Vishwanath, E. Berg, and J. Y. Lee, Fermionic Monte Carlo Study of a Realistic Model of Twisted Bilayer Graphene, Phys. Rev. X **12**, 011061 (2022).

[63] G. Pan, X. Zhang, H. Li, K. Sun, and Z. Y. Meng, Dynamical properties of collective excitations in twisted bilayer graphene, Phys. Rev. B **105**, L121110 (2022).

[64] X. Zhang, G. Pan, X. Y. Xu, and Z. Y. Meng, Fermion sign bounds theory in quantum Monte Carlo simulation, Phys. Rev. B **106**, 035121 (2022).

[65] X. Zhang, K. Sun, H. Li, G. Pan, and Z. Y. Meng, Superconductivity and bosonic fluid emerging from moiré flat bands, Phys. Rev. B **106**, 184517 (2022).

[66] X. Zhang, G. Pan, B.-B. Chen, H. Li, K. Sun, and Z. Y. Meng, Polynomial sign problem and topological Mott insulator in twisted bilayer graphene, Phys. Rev. B **107**, L241105 (2023).

[67] B.-B. Chen, Y. D. Liao, Z. Chen, O. Vafek, J. Kang, W. Li, and Z. Y. Meng, Realization of topological Mott insulator in a twisted bilayer graphene lattice model, Nat. Commun. **12**, 5480 (2021).

[68] X. Lin, B.-B. Chen, W. Li, Z. Y. Meng, and T. Shi, Exciton Proliferation and Fate of the Topological Mott Insulator in a Twisted Bilayer Graphene Lattice Model, Phys. Rev. Lett. **128**, 157201 (2022).

[69] M. Huang, Z. Wu, X. Zhang, X. Feng, Z. Zhou, S. Wang, Y. Chen, C. Cheng, K. Sun, Z. Y. Meng, and N. Wang, Intrinsic nonlinear Hall effect and gate-switchable Berry curvature sliding in twisted bilayer graphene, arXiv:2212.12666.

[70] H. Ritsch, P. Domokos, F. Brennecke, and T. Esslinger, Cold atoms in cavity-generated dynamical optical potentials, Rev. Mod. Phys. **85**, 553 (2013).

[71] R. Verresen, M. D. Lukin, and A. Vishwanath, Prediction of Toric Code Topological Order from Rydberg Blockade, Phys. Rev. X **11**, 031005 (2021).

[72] R. Samajdar, D. G. Joshi, Y. Teng, and S. Sachdev, Emergent $\mathbb{Z}_2$ Gauge Theories and Topological Excitations in Rydberg Atom Arrays, Phys. Rev. Lett. **130**, 043601 (2023).

[73] Z. Yan, X. Ran, Y.-C. Wang, R. Samajdar, J. Rong, S. Sachdev, Y. Qi, and Z. Y. Meng, Fully packed quantum loop model on the triangular lattice: Hidden vison plaquette phase and cubic phase transitions, arXiv:2205.04472.

[74] X. Ran, Z. Yan, Y.-C. Wang, J. Rong, Y. Qi, and Z. Y. Meng, Fully packed quantum loop model on the square lattice: Phase diagram and application for Rydberg atoms, Phys. Rev. B **107**, 125134 (2023).

[75] Y.-C. Wang, M. Cheng, W. Witczak-Krempa, and Z. Y. Meng, Fractionalized conductivity and emergent self-duality near topological phase transitions, Nat. Commun. **12**, 5347 (2021).

[76] H. Shao, Y. Q. Qin, S. Capponi, S. Chesi, Z. Y. Meng, and A. W. Sandvik, Nearly Deconfined Spinon Excitations in the Square-Lattice Spin-1/2 Heisenberg Antiferromagnet, Phys. Rev. X **7**, 041072 (2017).

[77] N. Ma, G.-Y. Sun, Y.-Z. You, C. Xu, A. Vishwanath, A. W. Sandvik, and Z. Y. Meng, Dynamical signature of fractionalization at a deconfined quantum critical point, Phys. Rev. B **98**, 174421 (2018).

[78] G.-Y. Sun, Y.-C. Wang, C. Fang, Y. Qi, M. Cheng, and Z. Y. Meng, Dynamical Signature of Symmetry Fractionalization in Frustrated Magnets, Phys. Rev. Lett. **121**, 077201 (2018).

[79] W. Wang, D.-C. Lu, X. Y. Xu, Y.-Z. You, and Z. Y. Meng, Dynamics of compact quantum electrodynamics at large fermion flavor, Phys. Rev. B **100**, 085123 (2019).

[80] Z. Yan, Y.-C. Wang, N. Ma, Y. Qi, and Z. Y. Meng, Topological phase transition and single/multi anyon dynamics of Z_2 spin liquid, npj Quantum Mater. **6**, 39 (2021).

[81] C. Zhou, Z. Yan, H.-Q. Wu, K. Sun, O. A. Starykh, and Z. Y. Meng, Amplitude Mode in Quantum Magnets via Dimensional Crossover, Phys. Rev. Lett. **126**, 227201 (2021).

[82] C. Zhou, M.-Y. Li, Z. Yan, P. Ye, and Z. Y. Meng, Evolution of dynamical signature in the X-cube fracton topological order, Phys. Rev. Res. **4**, 033111 (2022).

[83] Z. Yan and Z. Y. Meng, Unlocking the general relationship between energy and entanglement spectra via the wormhole effect, Nat. Commun. **14**, 2360 (2023).

[84] M. Song, J. Zhao, Z. Yan, and Z. Y. Meng, Reversing the Li and Haldane conjecture: The low-lying entanglement spectrum can also resemble the bulk energy spectrum, arXiv:2210.10062.

[85] O. K. Diessel, S. Diehl, N. Defenu, A. Rosch, and A. Chiocchetta, Generalized Higgs mechanism in long-range interacting quantum systems, arXiv:2208.10487.

[86] A. Chiocchetta, D. Kiese, C. P. Zelle, F. Piazza, and S. Diehl, Cavity-induced quantum spin liquids, Nat. Commun. **12**, 5901 (2021).

[87] E. Yusuf, A. Joshi, and K. Yang, Spin waves in antiferromagnetic spin chains with long-range interactions, Phys. Rev. B **69**, 144412 (2004).

[88] N. Defenu, Metastability and discrete spectrum of long-range systems, Proc. Natl. Acad. Sci. USA **118**, e2101785118 (2021).

[89] S. Birnkammer, A. Bohrdt, F. Grusdt, and M. Knap, Characterizing topological excitations of a long-range Heisenberg model with trapped ions, Phys. Rev. B **105**, L241103 (2022).

[90] K. Fukui and S. Todo, Order-n cluster Monte Carlo method for spin systems with long-range interactions, J. Comput. Phys. **228**, 2629 (2009).

[91] T. Horita, H. Suwa, and S. Todo, Upper and lower critical decay exponents of Ising ferromagnets with long-range interaction, Phys. Rev. E **95**, 012143 (2017).

[92] A. W. Sandvik and J. Kurkijärvi, Quantum Monte Carlo simulation method for spin systems, Phys. Rev. B **43**, 5950 (1991).

[93] A. W. Sandvik, Stochastic series expansion method with operator-loop update, Phys. Rev. B **59**, R14157 (1999).

[94] S. Toth and B. Lake, Linear spin wave theory for single-q incommensurate magnetic structures, J. Phys.: Condens. Matter **27**, 166002 (2015).

[95] J. L. van Hemmen, A note on the diagonalization of quadratic boson and fermion Hamiltonians, Z. Phys. B **38**, 271 (1980).

[96] C. J. Hamer, Z. Weihong, and P. Arndt, Third-order spin-wave

theory for the Heisenberg antiferromagnet, Phys. Rev. B **46**, 6276 (1992).

[97] W. Zheng, J. Oitmaa, and C. J. Hamer, Series studies of the spin-$\frac{1}{2}$ Heisenberg antiferromagnet at $t = 0$: Magnon dispersion and structure factors, Phys. Rev. B **71**, 184440 (2005).

[98] A. V. Syromyatnikov, Spectrum of short-wavelength magnons in a two-dimensional quantum Heisenberg antiferromagnet on a square lattice: Third-order expansion in 1/S, J. Phys.: Condens. Matter **22**, 216003 (2010).

[99] M. Kac, G. Uhlenbeck, and P. Hemmer, On the van der Waals theory of the vapor-liquid equilibrium. I. Discussion of a one-dimensional model, J. Math. Phys. **4**, 216 (1963).

[100] M. Antoni and S. Ruffo, Clustering and relaxation in Hamiltonian long-range dynamics, Phys. Rev. E **52**, 2361 (1995).

[101] R. Bachelard and M. Kastner, Universal Threshold for the Dynamical Behavior of Lattice Systems with Long-Range Interactions, Phys. Rev. Lett. **110**, 170603 (2013).

[102] E. Y. Loh, J. E. Gubernatis, R. T. Scalettar, S. R. White, D. J. Scalapino, and R. L. Sugar, Sign problem in the numerical simulation of many-electron systems, Phys. Rev. B **41**, 9301 (1990).

[103] G. Pan and Z. Y. Meng, Sign problem in quantum Monte Carlo simulation, arXiv:2204.08777.

[104] P. Bruno, Absence of Spontaneous Magnetic Order at Nonzero Temperature in One- and Two-Dimensional Heisenberg and *XY* Systems with Long-Range Interactions, Phys. Rev. Lett. **87**, 137203 (2001).

[105] Y.-Y. Jau, A. M. Hankin, T. Keating, I. H. Deutsch, and G. W. Biedermann, Entangling atomic spins with a Rydberg-dressed spin-flip blockade, Nat. Phys. **12**, 71 (2016).

[106] The diagonal and off-diagonal operators that sit on the same bond are still equally weighted even now, different weights and type bonds are assigned to different bonds, and this ensures that the loop update scheme does not need to be amended.